NON-LINEAR AEROELASTIC BEHAVIOR OF HIGHLY FLEXIBLE HALE WINGS

G.Romeo*, G.Frulla*, E.Cestino*, P.Marzocca**
***Politecnico di Torino, ****Clarkson University NY**

Keywords: *HALE Flutter Behaviour, Non-Linear Aeroelasticity, Limit Cycle Oscillations.*

Abstract

High aspect ratio aircrafts, such as High-Altitude Long-Endurance (HALE) UAVs, can experience large static deflections during normal flight operations that could severely reduce the flutter speed. At such speeds, Limit Cycle Oscillations (LCOs) may occur, reducing their operational life. A time-marching solver of a nonlinear aeroelastic model is proposed as a design analysis tool for highly flexible aircraft. Within this nonlinear aeroelastic model, moderate to large structural deflections and linear/non linear static and dynamic aeroelastic responses of such flexible aircraft can be properly considered. A geometrically consistent non-linear structural model is adopted based on Hodges and Dowell, including Da Silva second order geometrical non-linear terms. The structural model has been coupled with an unsteady aerodynamic model for an incompressible flow field, based on the Wagner aerodynamic indicial function, in order to obtain a non-linear aeroelastic model. This procedure enables one to expedite the calculation process. The influence of selected design aeroelastic parameters, such as tip deflection and stiffness ratio, is studied.
In addition to analytical and computational results, a high aspect-ratio wing model has been selected as a candidate for a feasibility experimental study and to validate the theoretical model. Preliminary results on a balsa wing model and theoretical comparisons are presented[1].

Nomenclature

a	= Elastic axis location.
b	= Semi-chord.
e	= Section mass center from elastic. Axis.
E	= Modulus of elasticity.
G	= Shear modulus.
U	= Free-stream velocity.
m	= Mass per unit length.
g	= Acceleration of gravity.
α	= Angle of attack.
I_η, I_ζ	= Vertical and chord-wise area. moments of inertia.
ρ	= Air density.
J	= Torsional stiffness constant.
ω_r	= Reference frequency.
L	= Wing span.
$\hat{\zeta}$	= Dimensionless in-plane generalized deformation.
$\hat{\eta}$	= Dimensionless out of plane generalized deformation.
$\hat{\phi}$	= Dimensionless torsional generalized deformation.
$\varepsilon_1, \varepsilon_2$	= Wagner function constants.
v, w, ϕ	= lag, flap displacements and torsional rotation.
$w_{3/4c}$	= Downwash velocity at ¾ chord.
F_v, F_w, M_ϕ	= Generic in-plane, out-of plane and aerodynamic moment resultant expressions.
EI_ζ, EI_η, GJ	= Bending and torsion rigidity.
$G'_v, G'_w G'_\phi$	= Added non-linear 2nd order terms.

1 General Introduction

Very low weight combined with high aspect ratio gives rise to slender and flexible wing structure. Such high degree of flexibility forces the designer to deal with specific phenomena not usually considered in classical aircraft definition proposing different design indications [8,9,10]. As we strive to reduce weight and raise performance levels using directional material, thus leading to an increasingly flexible aircraft, there is a need for reliable analysis tools, which model all the important characteristics of the fluid-structure interaction problem: aeroelastic instabilities always constrain the flight envelope and thus they have to be considered fundamental during the design process. One essential limitation of linearized analysis is that it can only provide information up to flight speed at which the aeroelastic instability occurs. Furthermore, these analyses are restricted to cases where the transient aeroelastic response amplitudes are small. Often this assumption is violated prior to the onset of instability. To study the behavior of aeroelastic systems near the point of instability, nonlinearities should be included. In recent years, studies of nonlinear fluid-structure interactions have been motivated by evidence that nonlinear effects in aeroelastic systems may be either favorable or unfavorable or a combination of both. For HALE UAVs it has been shown [3-4] that nonlinearities could induce Limit Cycle Oscillations (LCOs) even below the nominal flutter velocity. Whether such nonlinear effects are favorable or not will depend very much on the particular circumstances and parameters involved. Nonetheless it is clear that nonlinear effects often lead to LCO, which in turn, even if not catastrophic in nature, can lead to fatigue damage. In their absence the alternative would be a catastrophic flutter and consequently structural failure. To achieve an efficient design of flexible airplanes, a better understanding of all the factors contributing to the occurrence and increase of the flutter instability boundary, as well as of those determining if the limit cycle oscillations are stable or unstable are required.

2 Aeroelastic Model

In this paper a geometrically non-linear moderate to large deflection structural model, based on [1] and modified according to the second order geometrical non-linear terms introduced in [15], has been coupled with an unsteady aerodynamic model for an incompressible flow field based on the Wagner indicial function [2,13,19]. The strain displacement relations are developed from an exact transformation between the deformed and undeformed coordinate systems. The wing is assumed to be clamped in the plane of symmetry and the equations of motion are obtained from Hamilton's principle. These equations are also valid for beams with a mass centroid axis offset from the elastic axis, non-uniform mass and stiffness section properties, and variable pre-twist. Terms up to second order have been retained in the final expression. Higher non-linear coefficients have been neglected assuming they would have a negligible effect on the system dynamics. Rotary inertia has been neglected according to the slender beam hypothesis. The effect of shear deformation has also been neglected. The resulting equations (1a-c) are valid to second-order for long, slender, homogeneous, isotropic beams undergoing moderate to large displacements. Such assumptions are consistent with [1] and the reader is referred to [1,15] and the references cited therein for further details. In Eqs. (1a-c) G'_v, G'_w, G'_ϕ are second order non-linear terms derived from Da Silva [15].

$$\begin{cases} EI_\zeta v''''+\left[\left(EI_\zeta - EI_\eta\right)\phi w''\right]'' + G'_v + m\ddot{v} = L_v \\ EI_\eta w''''+\left[\left(EI_\zeta - EI_\eta\right)\phi v''\right]'' + G'_w + m\ddot{w} + me\ddot{\phi} = L_w \\ -GJ\phi''+\left(EI_\zeta - EI_\eta\right)v''w''+ G'_\phi + mk_m^2\ddot{\phi} + me\ddot{w} = M_\phi \end{cases} \quad \text{(1a-c)}$$

In order to solve the system of governing equations and to study the subcritical and supercritical aeroelastic response as well as the flutter boundaries, the introduction of a small dynamic perturbation about a non-linear static

equilibrium is applied. In-plane, out-of-plane and torsional deformations (v, w, ϕ) are considered to be a summation of the static and dynamic components in the undeformed reference system. The deflections are shown below:

$$\begin{aligned} v &= v_s + \bar{v} \\ w &= w_s + \bar{w} \\ \phi &= \phi_s + \bar{\phi} \end{aligned} \qquad \text{(2a-c)}$$

where v_s , w_s , and ϕ_s are the static in-plane lagging, out-of-plane bending and torsion deformations due to the aeroelastic trim, corresponding to a specific flight condition, respectively. The deformed beam scheme used in the present model is reported in Figure 1.

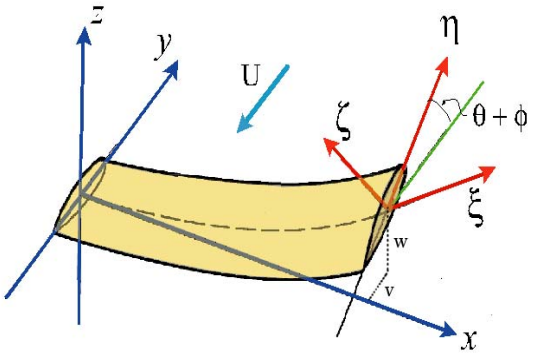

Fig. 1. *Wing reference system*

A moderate/large deflections small perturbations approximation has been introduced and the static variables are considered only x dependent. The dynamic deformations $\bar{v}, \bar{w}, \bar{\phi}$ are time and space dependent. Using modal analysis techniques, the solution of the problem can be expressed as:

$$\begin{aligned} v(x,t) &= v_s + \sum_{1}^{N_v} \zeta_i(t) v_i(x) \\ w(x,t) &= w_s + \sum_{1}^{N_w} \eta_i(t) w_i(x) \\ \phi(x,t) &= \phi_s + \sum_{1}^{N_\phi} \beta_i(t) \phi_i(x) \end{aligned} \qquad \text{(3a-c)}$$

The form of the solution is independent of the trial functions employed to discretize the system, but the proximity of the discrete system to the original one is dependent on selection of the functions. A well chosen set of trial functions can accurately represent the original continuous system in terms of a few discrete coordinates. Previous investigations on cantilever beams [14], using uncoupled mode shapes for flap-lag-torsion stability analysis, indicated that results would be accurate with as few as one or two modes. The example presented in this paper is obtained using six modes (two for each degree-of-freedom) with mode shapes derived from a vibrating uniform cantilever beam. The partial differential equations governing the dynamics of the flexible beam [1,6,9,10,15] were reduced to a system of ordinary differential equations using a series discretization technique [12], along with Galerkin's method, to obtain the aeroelastic governing equations. Substituting Eqs. (2a-c) into Eqs. (1a-c) it is possible to identify two sets of governing equations: a static aeroelastic equilibrium system and a perturbed dynamic system. The static equilibrium non-linear system can be expressed as:

$$\begin{cases} EI_\zeta v_s'''' + \left[\left(EI_\zeta - EI_\eta \right) \phi_s w_s'' \right]'' + G_{vs}' = F_v \\ EI_\eta w_s'''' + \left[\left(EI_\zeta - EI_\eta \right) \phi_s v_s'' \right]'' + G_{ws}' + mg = F_w \\ -GJ\phi_s'' + \left(EI_\zeta - EI_\eta \right) v_s'' w_s'' + G_{\phi s}' + mge = F_\phi \end{cases} \qquad \text{(4a-c)}$$

where $G_{vs}', G_{ws}', G_{\phi s}'$ are counterparts of the terms derived from [15] for the static equilibrium case. Given a free-stream velocity U and an angle-of-attack α , the static displacements v_s , w_s , ϕ_s for the corresponding trim condition can be computed. Notice that, in the perturbed dynamic system, the static configuration will couple with the dynamic components through the non-linear terms.
Introducing the variables $\hat{x} = x/L, \hat{w} = \hat{w}(\hat{x})$, $\hat{v} = \hat{v}(\hat{x})$, $\hat{\beta} = \hat{\beta}(\hat{x})$, a dimensionless form of the dynamic governing equations can be cast as:

$$\Gamma\Omega_h\sum_1^{N_v}\hat{\zeta}_i\hat{v}_i''''+\Omega_h(\Gamma-1)\left[\phi_s\sum_1^{N_w}\hat{\eta}_i\hat{w}_i''+\frac{w_s''}{b}\sum_1^{N_\phi}\hat{\beta}_i\hat{\phi}_i+\sum_1^{N_\phi}\hat{\beta}_i\hat{\phi}_i\sum_1^{N_w}\hat{\eta}_i\hat{w}_i''\right]''$$

$$+\hat{G}_v'+\sum_1^{N_v}\ddot{\hat{\zeta}}_i\hat{v}_i=\hat{L}_v$$

$$\Omega_h\sum_1^{N_w}\hat{\eta}_i\hat{w}_i''''+\Omega_h(\Gamma-1)\left[\phi_s\sum_1^{N_w}\hat{\zeta}_i\hat{v}_i''+\frac{v_s''}{b}\sum_1^{N_\phi}\hat{\beta}_i\hat{\phi}_i+\sum_1^{N_\phi}\hat{\beta}_i\hat{\phi}_i\sum_1^{N_w}\hat{\zeta}_i\hat{v}_i''\right]''+$$

$$+\hat{G}_w'+\sum_1^{N_v}\ddot{\hat{\eta}}_i\hat{w}_i+x_\alpha\sum_1^{N_\phi}\ddot{\hat{\beta}}_i\hat{\phi}_i=\hat{L}_w$$

$$-\Omega_\alpha\sum_1^{N_\phi}\hat{\phi}_i''\hat{\beta}_i+\Omega_h(\Gamma-1)\left[\frac{v_s''}{b}\sum_1^{N_w}\hat{\eta}_i\hat{w}_i''+\frac{w_s''}{b}\sum_1^{N_v}\hat{\zeta}_i\hat{v}_i''+\sum_1^{N_w}\hat{\eta}_i\hat{w}_i''\sum_1^{N_v}\hat{\zeta}_i\hat{v}_i''\right]+$$

$$+\hat{G}_\phi'+r_\alpha^2\sum_1^{N_\phi}\ddot{\hat{\beta}}_i\hat{\phi}_i+x_\alpha\sum_1^{N_w}\ddot{\hat{\eta}}\hat{w}=\hat{M}_\phi$$

(5a-c)

where prime refers to differentiation with respect to the dimensionless coordinate along the span. The terms $\hat{G}_v',\hat{G}_w',\hat{G}_\phi'$ couple the equations through torsional stiffness, even if $\Gamma\left(\equiv EI_\zeta/EI_\eta\right)=1$. Their full expressions can be found in [9,10]. The dimensionless parameters introduced in the Eqs. (5) are expressed as:

$$\Omega_h\equiv\frac{EI_\eta}{m\omega_r^2L^4},\Gamma=\frac{EI_\zeta}{EI_\eta},x_\alpha\equiv\frac{e}{b},\Omega_\alpha\equiv\frac{GJ}{m\omega_r^2b^2L^2},$$

$$r_\alpha^2\equiv\frac{mk_m^2}{mb^2},k\equiv\frac{\omega_rb}{U},\mu\equiv\frac{m}{\pi\rho b^2},a$$

(6a-h)

The unsteady aerodynamic forces can be obtained using Wagner's indicial function in Duhamel integral form [11,13] as reported in Eqs (7a-b).

$$L=\pi\rho b^2\left[\ddot{w}+U\dot{\phi}-ba\ddot{\phi}\right]-$$

$$-2\pi\rho Ub\left[w_{3/4c}(0)\Phi(t)+\int_0^t\frac{dw_{3/4c}}{d\sigma}\Phi(t-\sigma)d\sigma\right]$$

$$M_\phi=-2\pi\rho Ub^2(0.5+a)\left[w_{3/4c}(0)\Phi(t)+\int_0^t\frac{dw_{3/4c}}{d\sigma}\Phi(t-\sigma)d\sigma\right]+$$

$$+ab\rho\pi b^2\left(\ddot{w}-ba\ddot{\phi}\right)-\rho\pi Ub^2(0.5-a)b\dot{\phi}-\frac{\rho\pi b^4}{8}\ddot{\phi}$$

(7a-b)

where $\Phi(\tau)$ is the Wagner's function and a is the offset of the elastic axis position from the mid-chord, positive aft. Approximate expressions of the Wagner's function have been derived and the R.T. Jones approximation has been used [22] in the present application such as:

$$\Phi(\tau)=1-A_1e^{-b_1\tau}-A_2e^{-b_2\tau},\ (\tau>0)\qquad(8)$$

where the coefficients are: $A_i(0.165;0.335)$ and $b_i(0.0455;0.300)$. Due to the existence of the integral terms in the aerodynamic integro-differential equations [13], it is cumbersome to integrate them numerically. However, applying properties of the integration by parts, and introducing the variables [2,19,9,10]:

$$W_1=\int_0^t we^{-\varepsilon_1(t-\sigma)}d\sigma\ ,\ W_2=\int_0^t we^{-\varepsilon_2(t-\sigma)}d\sigma$$

$$W_3=\int_0^t\phi e^{-\varepsilon_1(t-\sigma)}d\sigma\ ,\ W_4=\int_0^t\phi e^{-\varepsilon_2(t-\sigma)}d\sigma$$

(9)

the airloads can be rewritten in general form containing just differential operators leading to a state-space form.

$$\hat{L}=\hat{C}_1\ddot{\hat{w}}+\hat{C}_2\dot{\hat{w}}+\hat{C}_3\hat{w}+\hat{C}_4\ddot{\hat{\phi}}+\hat{C}_5\dot{\hat{\phi}}+\hat{C}_6\hat{\phi}+$$

$$+\hat{C}_7\hat{W}_1+\hat{C}_8\hat{W}_2+\hat{C}_9\hat{W}_3+\hat{C}_{10}\hat{W}_4+\hat{F}_0$$

$$\hat{M}_\phi=\hat{D}_1\ddot{\hat{w}}+\hat{D}_2\dot{\hat{w}}+\hat{D}_3\hat{w}+\hat{D}_4\ddot{\hat{\phi}}+\hat{D}_5\dot{\hat{\phi}}+$$

$$+\hat{D}_6\hat{\phi}+\hat{D}_7\hat{W}_1+\hat{D}_8\hat{W}_2+\hat{D}_9\hat{W}_3+\hat{D}_{10}\hat{W}_4+\hat{P}_0$$

(10a-b)

where the coefficients $\hat{C}_i$ and $\hat{D}_i$ are functions of the elastic axis location a, the reduced frequency k, the mass parameter μ and the unsteady indicial function coefficients. F_0 and P_0 are the aerodynamic loads due to initial conditions. Their expressions can be found in [9]. The dimensionless state vector $\{X\}=\{x_1,...,x_{20}\}^T$ become function of the displacement variables and the additional aerodynamic lag states as:

$$\begin{aligned}
&\hat{x}_1=\hat{\zeta}_1,\ \hat{x}_2=\hat{\zeta}_2,\ \hat{x}_3=\hat{\eta}_1,\ \hat{x}_4=\hat{\eta}_2,\\
&\hat{x}_5=\hat{\beta}_1,\ \hat{x}_6=\hat{\beta}_2,\ \hat{x}_7=\hat{\varsigma}_1,\ \hat{x}_8=\hat{\varsigma}_2,\\
&\hat{x}_9=\hat{\eta}_1,\ \hat{x}_{10}=\hat{\eta}_2,\ \hat{x}_{11}=\hat{\beta}_1,\ \hat{x}_{12}=\hat{\beta}_2,\\
&\hat{x}_{13}=\hat{W}_{11},\ \hat{x}_{14}=\hat{W}_{21},\ \hat{x}_{15}=\hat{W}_{31},\ \hat{x}_{16}=\hat{W}_{41},\\
&\hat{x}_{17}=\hat{W}_{12},\ \hat{x}_{18}=\hat{W}_{22},\ \hat{x}_{19}=\hat{W}_{32},\ \hat{x}_{20}=\hat{W}_{42}
\end{aligned} \tag{11}$$

Applying the convolution integral property [2,19], the remaining constraint equations can be derived in order to complete the system. Constraint equations obtained from Wagner's indicial theory are expressed as:

$$\begin{aligned}
&\dot{\hat{x}}_{13}=\hat{x}_9-\frac{\hat{\varepsilon}_1}{k}\hat{x}_{13},\ \dot{\hat{x}}_{14}=\hat{x}_9-\frac{\hat{\varepsilon}_2}{k}\hat{x}_{14},\\
&\dot{\hat{x}}_{15}=\hat{x}_{11}-\frac{\hat{\varepsilon}_1}{k}\hat{x}_{15},\ \dot{\hat{x}}_{16}=\hat{x}_{11}-\frac{\hat{\varepsilon}_2}{k}\hat{x}_{15},\\
&\dot{\hat{x}}_{17}=\hat{x}_{10}-\frac{\hat{\varepsilon}_1}{k}\hat{x}_{17},\ \dot{\hat{x}}_{18}=\hat{x}_{10}-\frac{\hat{\varepsilon}_2}{k}\hat{x}_{18},\\
&\dot{\hat{x}}_{19}=\hat{x}_{12}-\frac{\varepsilon_1}{k}\hat{x}_{19},\ \dot{\hat{x}}_{20}=\hat{x}_{12}-\frac{\varepsilon_2}{k}\hat{x}_{20},
\end{aligned} \tag{12}$$

The aeroelastic system can finally be written in a state-space form as:

$$\{\dot{X}\}=[A]_{LIN}\{X\}+[G]_{NLIN}\{X\} \tag{13}$$

where $[A]_{LIN}$ is a matrix containing linear terms that are functions of the equilibrium solution and $[G]_{NLIN}$ is a matrix containing only non-linear terms. Flutter speed & frequency are defined by [13] as the lowest airspeed and corresponding frequency at which a given structure flying in a specific atmosphere will exhibit sustained simple harmonic oscillations. Flutter condition is a borderline situation or neutral stability due to the fact that small motions must be stable at a speed below linear flutter speed, whereas divergent oscillations occur in a range of speed above flutter speed. Linear flutter speed calculations can be performed setting the matrix $[G]_{NLIN}$ equal to zero. The stability of motion about the equilibrium operating condition is determined by the eigenvalues of the $[A]_{LIN}$ matrix. The reduced linear perturbation system originates a linear approximation of the behaviour of the system in the neighborhood of the static equilibrium point with the possibility of calculating a flutter speed for each trim condition. Linear flutter speed can be computed assuming the equilibrium static configuration as zero with no coupling effect computing eigenvalues of $[A(.....,v_s=0,w_s=0,\phi_s=0)]_{LIN}$. Including equilibrium terms, non-linear flutter speed calculations can be performed computing eigenvalues of $[A(.....,v_s\neq 0,w_s\neq 0,\phi_s\neq 0)]_{LIN}$ [9,10,20]. The system response is then analyzed via time marching integration by the non-linear Mathematica® solver. Linear integration, maintaining $[G]_{NLIN}=0$, or non-linear integration, $[G]_{NLIN}\neq 0$, can be carried out to investigate the post-flutter behaviour.

3 Results and Discussion

3.1 Linear and nonlinear Flutter

To validate the proposed non-linear aeroelastic model, Patil and Hodges [3,4] and Tang and Dowell [5] models have been considered. The present results are in very close agreement with [3-5]. High-aspect-ratio wings undergo large deflections for relatively low aerodynamic loadings as compared to low-aspect-ratio wings, and the natural frequencies of the high-aspect-ratio wings are quite low. Under aerodynamic loading the wing exhibits large static deflections, that is, effectively is a curved wing, for which a non-linear coupling between torsion and lagging bending occurs [1].

The classical linear flutter speed, obtained by linearizing the non-linear model about a zero deflection steady state, is calculated first. Throughout this paper it will be referred to as VFLEC that is: "flutter velocity in linear equilibrium condition". Linearizing the system about a deformed steady state, the perturbed motion is influenced by the chosen equilibrium point. The reduced linear perturbation system generates a linear approximation of the behavior of the system in the neighborhood of the static equilibrium point, with the possibility of calculating a flutter speed for each condition. In this case, the flutter speed is identified throughout this paper as VFNLEC that is: "flutter velocity in non-linear equilibrium condition". To appreciate the importance of the non-linear effect of static deformation, a preliminary analysis was carried out introducing static deformations relative to imposed load distributions. Structural and aeroelastic characteristics of the wing were investigated by linearizing the problem about a non-linear statically deformed state. In Figure 2 the first four modes obtained by NASTRAN linear and non-linear analysis are presented for the same beam. The modal content of the undeflected wing structure at zero speed consists of six modes: first and third modes ($\omega_1/\omega r$=0.022, ω_3/ω_r=0.1386) are typical flapping-bending modes, second and fifth modes (ω_2/ω_r=0.0983, ω_5/ω_r=0.5836) are typical lagging-bending modes, finally fourth and sixth modes (ω_4/ω_r=0.3052, ω_6/ω_r=0.9151) are two torsional modes. It is clear from both, the theoretical and FE analysis, that the variation in frequency is mostly due to lagging/torsion coupling. For even higher deformations there is further decrease in the torsional/lagging bending frequency, pushing the mode closer to the first bending mode. There is also a further decrease in the flutter speed, therefore the flutter characteristics of a deflected wing are very different from those of a straight wing due to the structural geometric nonlinearities. A subsequent flutter analysis has been performed and preliminary flutter calculations for a typical slender wing configuration are reported. The VFLEC has been determined first and correspond to the stability characteristics of the unloaded, undeformed wing. Some preliminary numerical results are presented in the following, referring to the wing data reported in [3]. A VFLEC of about 0.9 has been obtained showing a good correlation with results reported in [3]. The aeroelastic model has been than linearized about nonlinear steady states corresponding to different static load conditions. This analysis gives a more realistic prediction of the stability of the wing.

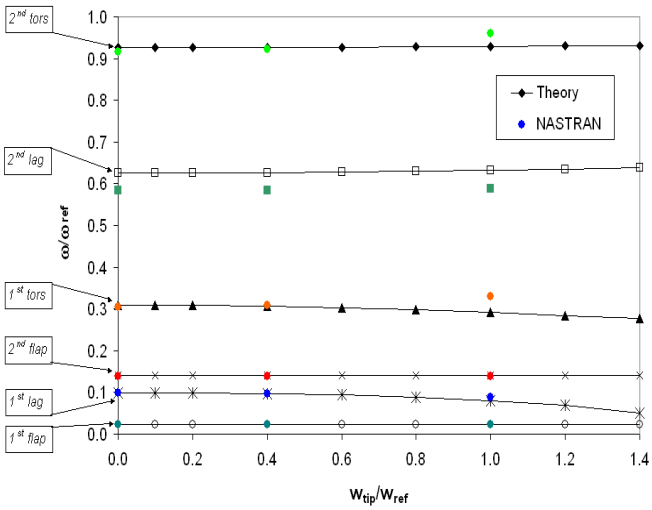

Fig. 2. *NASTRAN and theoretical frequency content.*

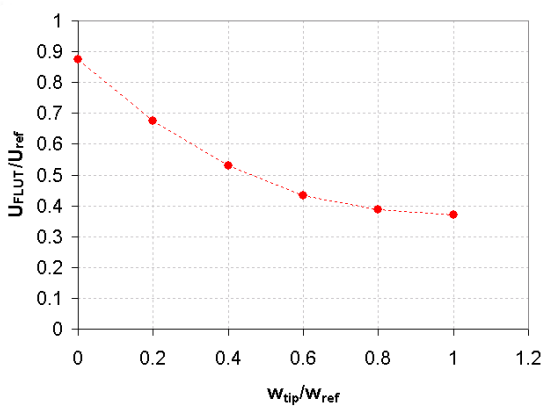

Fig. 3. *Tip deflection effect*

It has been pointed out [3,8], that the flutter instability is greatly influenced by a static tip displacement. Similar results has been obtained for the case under study. Considering, for example, the case of a static tip displacement ratio w_{tip}/w_{ref} of 0.4, the VNFLEC reduce to

0.5 and, for w_{tip}/w_{ref} of 1, VNFLEC become lower than 0.4 showing a reduction of about 47-54%. The VNFLEC behavior as a function of the tip displacement ratio is reported in Figure 3. This is an important fact to consider when analyzing the non-linear aeroelastic behavior of such wings. Another design indication derived from [8] and confirmed by results published in [9] shows as the stiffness ratio between in-plane stiffness EI_ζ and out-of-plane stiffness EI_η could play an important role in increasing the flutter boundaries; in [8,9] has been pointed out the positive effect of increased flutter speed when an higher value of the stiffness ratio is introduced in the airplane structure design. The static wing deflection, previously considered, was not the real deflection obtained solving the equilibrium system in Eqs. (6a-c). For this reason a change in the calculation procedure has to be introduced. A correct procedure to compute the critical flutter speed can be performed according to the scheme in Figure 4. As an example, if we consider that at every speed a level flight condition has to be satisfied, then the flutter speed and frequency could be obtained as follows: 1) choose a flight speed and the correct angle-of-attack to satisfy the vertical equilibrium condition 2) calculate the static equilibrium deformed shape at the flight speed, 3) linearize about the deformed shape, 4) calculate the eigenvalues of the linearized system, 5) check for stability, if stable, increase the flight speed and repeat all of the preceding steps until instability speed is reached.

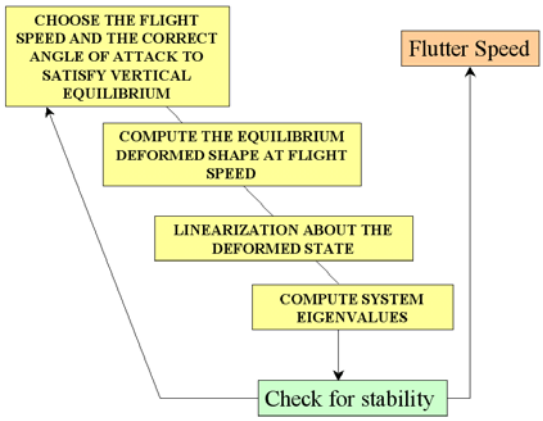

Fig. 4. *Flutter speed calculation*

A similar procedure has been suggested by Patil [15] and applying this approach, a higher VFNLEC flutter speed could be obtained.

3.2 Post-Flutter Behaviour

The flutter results obtained in the previous section give the velocity at the onset of flutter. These flutter results imply that small disturbances will grow exponentially for velocities higher than the flutter speed. However, as the amplitude of oscillations grows, additional non-linear stiffness is produced. Thus, the vibrations do not grow to infinity but instead converge to a limit cycle oscillation (LCO). The amplitude of the LCO gives an idea of the amount of stress/strain on the structure therefore its study could be useful in analysis and design. The amplitude of the LCO can only be determined by time-marching the non-linear governing equations of the aeroelastic system, while qualitative studies of the character of the flutter boundary, that is the identification of a stable or unstable LCO, can be done, for example, via a Lyapunov based approach proposed in [21]. In this paper, the effect of nonlinearities on the post-flutter behavior has been investigated by considering a small initial disturbance and by analyzing the response via time marching integration scheme using the non-linear Mathematica® solver. To provide a better understanding of how nonlinearities, incorporated in the aeroelastic model, affect the response of the system, Figure 5 shows the time histories for the tip deflections at a speed higher then the flutter speed. The linear system show the typical unstable behavior with growing amplitudes as time unfolds. It clearly appears that the nonlinearities constrain the system to a limit cycle. For the fully nonlinear system LCOs are present above the non-linear flutter speed, as presented in Figure 6. Herein the in-plane and out-of-plane wing tip deflections reach a stable LCO within 18 sec. This behavior is also representative of the torsional deflection. Considering the effect of steady-state system configuration in the flutter and post-flutter behavior, we have assumed a

level flight condition that is verified at every speed.

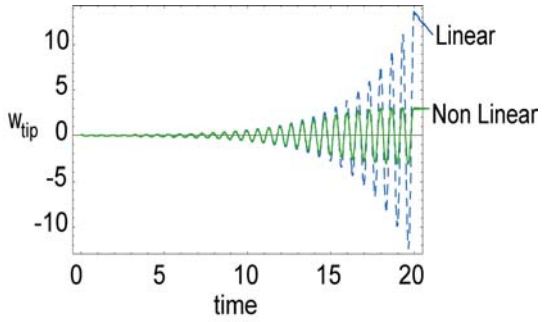

Fig. 5. *Time histories of linear and nonlinear systems*

A VFNLEC of 0.6 was computed considering lagging, flapping and torsional static deformations and a VFLEC of 0.862 was determined for the case of an undeformed steady state equilibrium. After the non-linear flutter velocity an LCO was recorded. This clearly demonstrates the importance of incorporating geometric nonlinearities in the aeroelastic model because it not only affects the flutter speed, but also the post-flutter aeroelastic behavior.

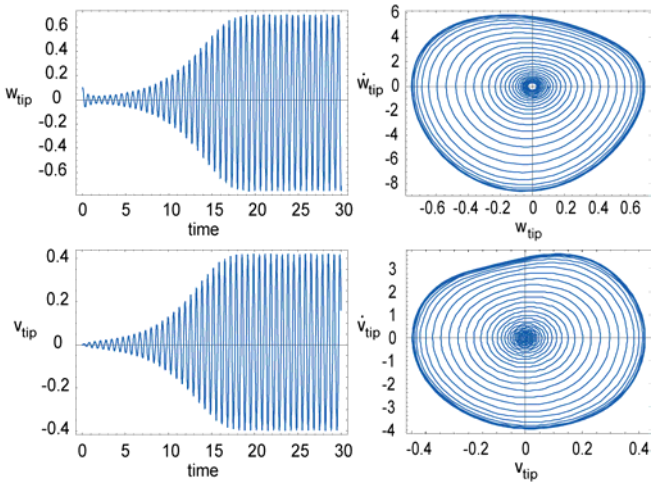

Fig. 6. *Post-flutter behaviour*

4. Experiments and Numerical Results

In addition to analytical and computational results, experiments will be conducted on a high-aspect-ratio wing model with a slender body at the tip in order to validate the theoretical model previously described. A preliminary experimental study has been conducted on a balsa wood wing. Three aspect-ratio wings have been tested both below and above VFLEC and VFNLEC flutter speeds. As highlighted in [5], a hysteresis phenomenon was also found during the test, confirming that these highly flexible wings exhibit a subcritical, unstable LCO behavior. Above the non-linear flutter speed, a stable LCO occurs. This LCO remains stable and its amplitude increases as the speed increases (Fig 11). In the descending speed phase, the LCO remain stable even below the VFNLEC flutter speed. In all the experiments a magnetic sensor, Vernier MB-BTA (200 samples per second), was used to record the variation in magnetic field produced by a rare-heart magnet (low mass, high magnetic field) attached to the wing (Fig 7). Magnetic field is correlated with displacement, so it was possible to record tip displacement and LCO post-flutter behavior. The wings were mounted, through a variable angle-of-attack support, vertically into the wind-tunnel to overcome the effect of gravity loading (Fig 7). The main characteristics of the tested wing in terms of dimensionless aeroelastic parameters for the balsa wing are reported in the Table 1.

k	μ	Ω_h	Ω_α	Γ	x_α	r_α^2	a
variable	10.8064	0.40303	210.946	96.77	0	0.5327	0

Table 1

Experimental tests show a flutter speed ratio of U_{flut}/U_{ref}=0.514 in the increasing velocity phase and a flutter speed of about 0.468 in the decreasing velocity phase. A static deflection of approximately 65 mm at the flutter velocity was recorded, confirming the theoretical prediction of the deformed equilibrium (Fig.7). Theoretical results have shown the non-linear behavior of these high-aspect-ratio wings. A linear flutter speed VFLEC of about 0.871 was computed using the dynamic perturbation approach explained in the previous section (Fig.8a,b). The linear value is quite far from the flutter speed recorded during the experiment. Introducing an imposed static

deflection with a tip displacement of 65mm, a non-linear flutter speed ratio of approximately 0.5 was computed by the theoretical model (Figs 10a-b), showing a good correlation with the experimental results.

Fig. 7. *Balsa wing static deflection*

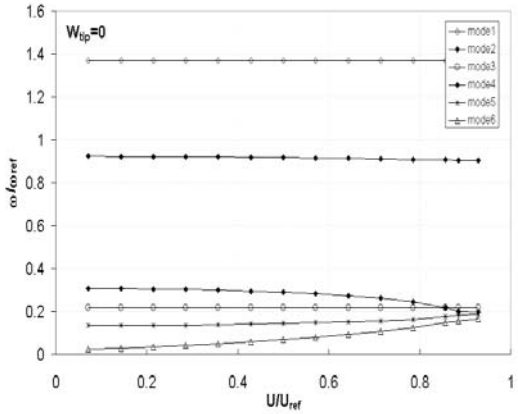

Fig. 8a. *Undeflected balsa wing*

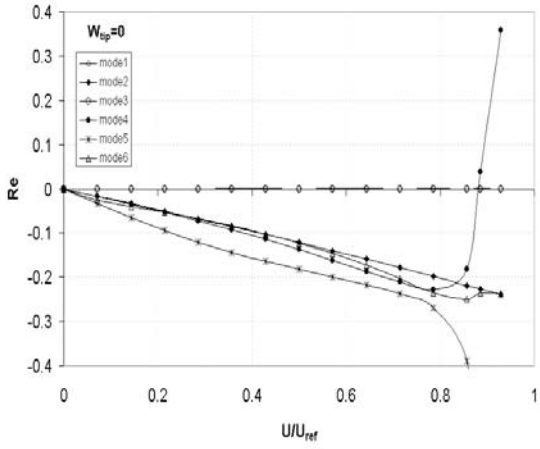

Fig. 8b. *Undeflected balsa wing computations*

Figures 8, 9, show a graphical representation of the perturbation equations eigenvalue analysis, in the form of real eigenvalues Re(λi) (damping) versus the flow velocity. When the real part of the eigenvalues become positive we can recognize the flutter speed for the two cases of linear and non-linear equilibrium.

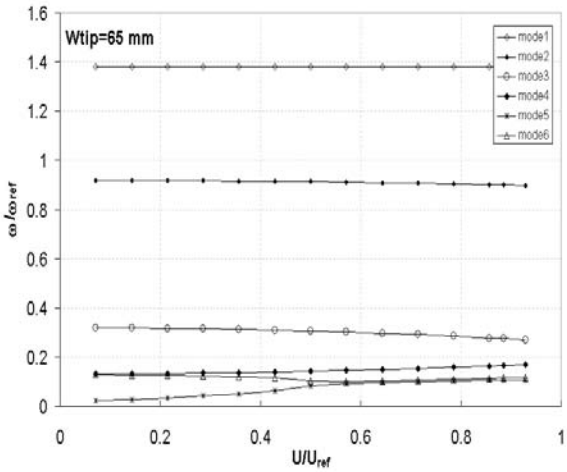

Fig. 9a. *Deflected (65mm) balsa wing*

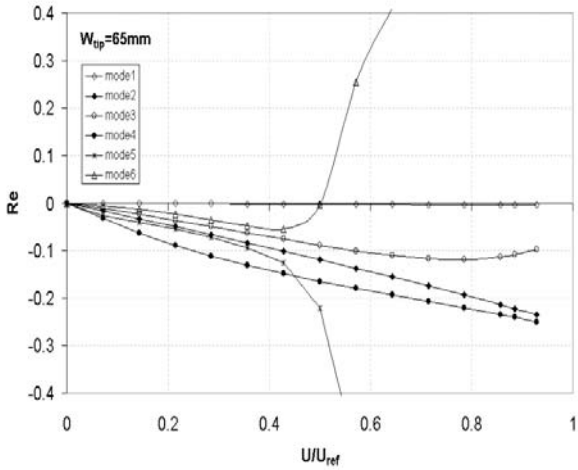

Fig. 9b. *Deflected (65mm) balsa wing computations*

A clear flutter and LCO response has also been observed in the present wind tunnel tests. The LCO results characterizing the post flutter behaviour show hysteretic response with increasing and decreasing flow velocity. As shown in [5], this phenomena is caused by both structural and aerodynamic nonlinearity due to separations at high angle-of-attack. The evolution of LCOs at speeds higher than non-linear flutter speed was studied for different speeds and angle-of-attacks. One of the measured time histories for the wing at an angle-of-attack of 8 degrees is shown in Figure 10. A second experimental model is also

proposed. The advanced stereo-lithography model has been constructed and will be tested in the low speed wind tunnel at Clarkson University [9,10]. Results of this advanced model will be presented elsewhere. The wing is rectangular, untwisted, and flexible in flap, lag and torsion. An extremely fine aerodynamic shape is obtained. The wing is composed by several pieces of NACA 0015 resin parts supported by a metallic bar. Resin parts are only bonded to the metallic bar leaving microgaps between the resin parts in order to reduce torsional stiffness.

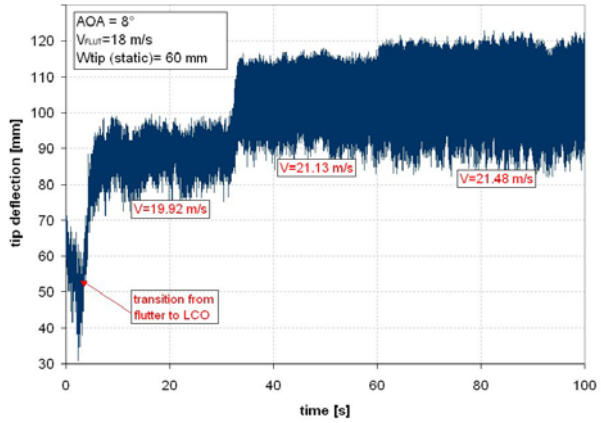

Fig. 10a. *Balsa wing time histories and recorded LCOs*

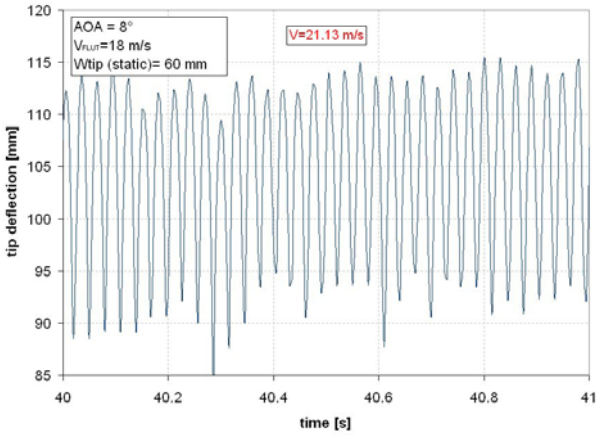

Fig. 10b. *Balsa wing time histories and recorded LCOs*

5. Conclusion

High Altitude Long Endurance (HALE) aircrafts aero-structural interactions are presented and defined. An advanced flutter calculation is presented and applied to the aeroelastic performance of slender structure, as used in HALE wings. The effect of the deflected equilibrium configurations, obtained by non-linear approximation, is taken into consideration when solving the aeroelastic small motions system. The Galerkin approach in reduced form is considered as an analytical tool used to perform the calculations. Aerodynamic loads are derived according to the Wagner function approach and are simplified in these preliminary calculations. Post-flutter behaviour and LCO evolution has been studied using a time-marching approach by means of Mathematica® non-linear solver. In addition to analytical and computational results, a high-aspect-ratio wing model has been selected for a feasibility study case and for validation of the theoretical model. Preliminary tests have been conducted showing a good correlation between the theoretical model and the experimental results. More experiments are being conducted on an advanced stereo-lithography model.

Reference

[1] Hodges DH, Dowell EH. Non-linear Equations of Motion for the Elastic Bending and Torsion of Twisted Non Uniform Rotor Blades. *NASA TN D-7818*, 1974.

[2] Sedaghat A, Cooper JE, Wright JR. Prediction of Non Linear Aeroelastic Instabilities. *Proc. ICAS 2000 Congress*, Harrogate UK, 28 August-1 September, 2000.

[3] Patil MJ, Hodges DH. On the Importance of Aerodynamic and Structural Geometrical Non-linearities in Aeroelastic Behavior of High-Aspect-Ratio Wings. *Journal of Fluids and Structures*, Vol. 19, pp. 905–915, 2004.

[4] Patil MJ, Hodges DH. Limit-Cycle Oscillations in high-aspect-ratio wings. *Journal of Fluids and Structures*, Vol. 15, pp. 107-132, 2001.

[5] Tang D, Dowell EH. Experimental and Theoretical Study on Aeroelastic Response of High-Aspect-Ratio Wings. *AIAA Journal*, Vol. 39, No. 8, pp. 419-429, 2001.

[6] Houbolt JC, Brooks GW. Differential Equations of Motion for Combined Flapwise Bending, Chordwise Bending, and Torsion of Twisted Nonuniform Rotor Blades. *NACA Report 1346*.

[7] Romeo G, Frulla G, Cestino E, Corsino G. HELIPLAT: Design, Aerodynamic, Structural Analysis of Long-Endurance Solar-Powered

Stratospheric Platform. *Journal of Aircraft*, Vol. 41, No. 6, pp. 1505-1520, 2004.

[8] Frulla G. Aeroelastic Behavior of a Solar-Powered High-Altitude Long Endurance Unmanned Air Vehicle (HALE-UAV) Slender Wing. *Journal of Aerospace Engineering Part G Special Issue*, Vol. 218, pp.179-188, 2004.

[9] Cestino E. Design of very long-endurance solar powered UAV, *PhD Dissertation* Politecnico di Torino, Aerospace Dept. , Torino, 2006.

[10] Romeo G, Frulla G, Cestino E, Marzocca P, Tuzcu I. Nonlinear Aeroelastic Modeling and Experiments of Flexible Wings, *Proc. 47th AIAA/ASME/ASCE/AHS/ASC Structures, Structural Dynamics, Materials Conference*, Newport RI, 1-4 May, 2006.

[11] Librescu L, Chiocchia G, Marzocca P. Implications of Cubic Physical/Aerodynamic Non-linearities on the Character of the Flutter Instability Boundary. *International Journal of Non-linear Mechanics*, Vol. 38, pp. 173-199, 2003.

[12] Meirovitch L. *Fundamentals of Vibrations*. McGraw Hill, New York 2001.

[13] Bisplinghoff RL, Ashley H and Halfman RL. *Aeroelasticity*, Dover, New York 1996.

[14] Hodges DH, Ormiston RA. Non-linear Equations for Bending of Rotating Beams with Application to Linear Flap-Lag Stability of Hingeless Rotors. *NASA TM X-2770*, 1973.

[15] Crespo Da Silva MRM. Non-linear Flexural-Flexural-Torsional-Extensional Dynamics of Beams-I. Formulation. *International Journal of Solids and Structures*, Vol. 24, No. 12, pp. 1225-1234, 1988.

[16] Tang DM, Dowell EH. Experimental and Theoretical Study on Aeroelastic Response of High-Aspect-Ratio Wings. *AIAA Journal*, Vol 39, No. 8, August 2001.

[17] Patil MJ, Hodges DH. Cesnik CES. Nonlinear Aeroelasticity and Flight Dynamics of High-Altitude Long-Endurance Aircraft. *Journal of Aircraft,* Vol. 38, No.1, pp. 88-94, 2001.

[18] Timoshenko S. *Vibration problems in engineering*, Third Edition, D.Van Nostrand Company Inc, 1935.

[19] Lee BHK, Price SJ, Wing YS. Nonlinear aeroelastic analysis of airfoils: bifurcation and chaos. *Progress in Aerospace Sciences*, Vol. 3, pp. 205-334, 1999.

[20] Marzocca P, Librescu L, Chiocchia G. Aeroelastic Response of a 2-D Lifting Surfaces to Gust and Arbitrary Explosive Loading Signatures. *International Journal of Impact Engineering*, Vol. 25, No. 1, pp. 41-65, 2001.

[21] Dowell E, Edwards J, Strganac T. Nonlinear Aeroelasticity. *Journal of Aircraft*, Vol 40, No. 5, pp 857-874, 2003.

[22] Jones RT, The unsteady lift of a wing of finite aspect ratio. *NACA Rept 681*, 1940.